



## MODELING OF THE FLUID MECHANICS OF CRYOGENIC SPILLS ONTO THE SEA AND RADIATION FIELDS FROM SUBSEQUENT POOL FIRES DURING LNG MARITIME TRANSPORTATION

### Alan Silva Esteves

Pontifícia Universidade Católica do Rio de Janeiro  
Departamento de Engenharia Mecânica  
Rua Marquês de São Vicente 225, Gávea, 22453-900, Rio de Janeiro RJ  
e-mail: alan-esteves@esp.puc-rio.br

### José Alberto Reis Parise

Pontifícia Universidade Católica do Rio de Janeiro  
Departamento de Engenharia Mecânica  
Rua Marquês de São Vicente 225, Gávea, 22453-900, Rio de Janeiro RJ  
e-mail: parise@puc-rio.br

**Abstract.** *The paper innovatively connects both themes and implements them in a computer code. The spill/spreading considers the area of maximum pool poured onto the sea as well as the unloading and vaporization times of the cryogenic fluid. The flow is modeled for tear areas between 1 and 100 m<sup>2</sup>, forming semicircular pools. The fire thermal plume modeling assumes circular pools with diameters between 10 and 500 m, and the existence of combustion and intermittency zones. It also evaluates the axial variation of emissive power with height of the visible plume, the burning of fuel along the base of the fire, and the transport of thermal radiation emitted by gray gases and soot particles within the combustion zone, considering the emission and absorption in optically thin and thick regions of the plume.*

**Keywords:** *Liquefied Natural Gas (LNG), spill/scattering, turbulent diffusion pool fire, surface emissive power.*

## 1. INTRODUCTION

LNG carriers had its capacity scale of 125,000-180,000 m<sup>3</sup> raised significantly when the ‘Mozah’ first LNG carrier Q-max with 266,000 m<sup>3</sup>, was launched (QatarGas, 2008) and such scale have been currently raised questions about the construction of new LNG terminals. Spills are caused by punctures, due to accidents or intentional acts of terrorism, brought against broadsides of LNG carriers, and may result in pool fires alongside the stricken tanker (Sandia, 2008). Spill and combustion models are coupled to each other, and the semicircular diameter obtained with the first is then converted into a circular one and is fed as input data to the fire model, presenting plausible numerical results.

## 2. BRIEF LITERATURE OVERVIEW

### 2.1 LNG spill/spreading/vaporization modeling

Different types of flow regimes and pool formation considered spills from large carriers (Blanchat et al., 2011; MKOPSC, 2008), providing the unique physics of LNG spills and its peculiar chemical composition and cryogenic behavior, differently than the traditional hydrocarbons spills (Lehr, 2007). Relevant results can be reviewed and consolidated in a number of works and review papers, including MKOPSC (2008), Raj (2007a) and Sandia (2004). More recently, other works studied the consequences of large-scale LNG spills on water (Oka, 2010) and of LNG releases, pool formation and spreading, followed by pool fire radiant heat output and hazard distance calculation procedures. Hissong (2007) and FERC (2004), to name but a few, discussed the spreading and the evaporating of a pool of LNG on water, in terms of various flow regimes, such as (i) gravity-inertial regime, (ii) gravity-viscous regime and (iii) surface tension-viscous regime. For boiling on water surface three boiling regimes can be distinguished (Hissong, 2007): (i) nucleate boiling, (ii) transition boiling and (iii) film boiling.

### 2.2 Pool fire modeling

Pool fire models are currently available to predict heat fluxes at a given distance, ranging from punctual sources to field models, involving CFD, and can be divided into five main categories (Pula et al., 2005), namely: (i) punctual source flame (semi-empirical), Lees (1996); (ii) solid flame, Rew et al. (1998); (iii) integral, Vachon and Champion (1986); (iv) multi-zones, Fay (2006), TMS (2006), Raj (2007b) and (v) field (CFD), Johnson (1992). From all of the abovementioned types, multi-zone models for large scale pool fires and CFD pool fires applications (limited to small diameters pools) have turned out to be the focus of scientific and technical development nowadays.

### 2.2.1 Multi-zones models

Current models for pool fires simulation consider different regions of combustion within the apparent (visible) height of the flame (MKOPSC, 2008; Raj, 2007b; TMS, 2006; Fay, 2006), since it is recognized in the literature that, as the diameter increases, the thermal plume becomes to consist of distinct zones. The results have been validated quantitatively by Raj (2007b), Malvos and Raj (2006), TMS (2006), Fay (2006), Luketa-Hanlin (2006), Sandia (2004). For that reason, they have been chosen for the present work.

## 3. MATHEMATICAL MODEL

### 3.1 Semicircular pool spill/spreading

The sketched geometry of the damaged LNG carrier is presented in Fig. 1.

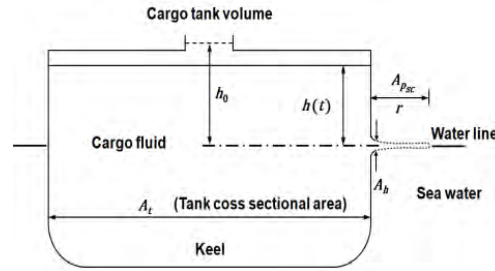


Figure 1. Membrane or prismatic cargo tank of a LNG carrier - Adapted from: Fay (2003)

#### 3.1.1 Model equations

Mass and linear momentum conservation equations are:

$$\dot{M} \equiv \frac{D}{Dt} \iiint_{V_m(t)} \rho_l dV_m(t) = 0 \quad (1)$$

$$\underbrace{\frac{D}{Dt} \iiint_{V_m(t)} \rho_l u_i dV_m(t)}_{\text{Rate of change of linear momentum}} = \underbrace{\iiint_{V_m(t)} \rho_l f_i dV_m(t)}_{\text{Body forces}} + \underbrace{\iiint_{V_m(t)} \frac{\partial}{\partial x_j} T_{ij} dV_m(t)}_{\text{Surface forces}} \quad (2)$$

where  $\dot{M}$  is the mass flow rate (kg/s),  $V_m(t)$  is the volume ( $\text{m}^3$ ) of a fluid material particle at a time  $t$  (s),  $\rho_l$  is the cargo cryogenic liquid mass density ( $\text{kg}/\text{m}^3$ ),  $u_i$  is the velocity (m/s) field vector of this particle,  $f_i$  is the resultant of body forces (N) acting on the particle,  $T_{ij}$  is the tensor of surface tensions ( $\text{N}/\text{m}^2$ ). The fluid is assumed as Newtonian with constant properties and its movement is governed by the Navier-Stokes equation, where  $P$  ( $\text{N}/\text{m}^2$ ) is the pressure,  $x$  is the distance (m),  $\lambda$  and  $\mu$  are the global and dynamic viscosities in  $\text{kg}/\text{m}\cdot\text{s}$ , such as:

$$\underbrace{\frac{D}{Dt}(\rho_l u_i)}_{\text{Total acceleration of the fluid material particle per unit of volume}} = \underbrace{\rho_l f_i}_{\text{Body forces per unit of volume}} - \underbrace{\frac{\partial P}{\partial x_i}}_{\text{Pressure forces per unit of volume}} + \underbrace{\left(\lambda + \frac{1}{3}\mu\right) \frac{\partial}{\partial x_j} \frac{\partial u_i}{\partial x_j}}_{\text{Maximum net convective effects experienced by the fluid viscosity per unit of volume}} + \underbrace{\mu \frac{\partial^2 u_i}{\partial x_i^2}}_{\text{Viscous forces per unit of volume}} \quad (3)$$

The spread of an evaporating LNG pool can be regarded essentially as an inviscid flow. After simplifications, Eq. (3) becomes  $-D(\rho_l u_i)/Dt \approx \partial P/\partial x_i$ . The cargo tank deployment is supposed to take place at atmospheric pressure without significant variation as the pool spreads, so  $\partial P/\partial x_i \approx 0$ . Since linear momentum is conserved, the Euler equation can be applied along a radial streamline (Fay, 2003, 2007). At each point of this line, to which  $u_i$  is tangent, the total acceleration of a fluid material particle,  $Du_i/Dt$ , spreads it within the pool following the motion. This movement is described by the Euler's material acceleration, where  $\delta_{ij}$  is the tensor of Kronecker's delta:

$$a_i \hat{e}_i = \frac{D}{Dt}(\rho_l u_i) \hat{e}_i = \frac{\partial u_i}{\partial t} \hat{e}_i + u_j \delta_{ij} \frac{\partial u_k}{\partial x_j} \hat{e}_k = \frac{\partial u_i}{\partial t} \hat{e}_i + u_j \frac{\partial u_i}{\partial x_j} \hat{e}_i \Rightarrow \frac{Du_i}{Dt} = \frac{\partial u_i}{\partial t} + u_j \frac{\partial u_i}{\partial x_j} \quad (4)$$

For this sort of nearly frictionless flow, Fay's (2003) model considers that it is possible to have an exact solution of the Euler's equation along a radial streamline, with a fluid material particle in the position  $r = |\mathbf{r}|$  in (m). It is supposed to have a movement at a fixed radial speed starting at the origin of the spill, and the equation that describes this movement is given in cylindrical coordinates by (Fay, 2003, 2007), such as:

$$a_i = \frac{Du_i}{Dt} = \frac{\partial u_i}{\partial t} + u_j \frac{\partial u_i}{\partial x_j} \Rightarrow \frac{Du}{Dt} = \frac{\partial u}{\partial t} + u \frac{\partial u}{\partial r} \quad (\text{on the streamline}) \quad (5)$$

Hoult (1972) developed a self-similar solution to Euler's equation along a radial streamline for an inertial-gravity spread, as follows (Fay, 2007), where  $\bar{\delta}$  is the average pool thickness (m) with  $\Delta$  being given by Eq. (7):

$$\frac{\partial u}{\partial t} + u \frac{\partial u}{\partial r} + g\Delta \frac{\partial \bar{\delta}}{\partial r} = 0 \quad (6)$$

$$\Delta = \frac{\rho_w - \rho_l}{\rho_w} \quad (7)$$

For a LNG slick, the length scale is very small when compared to a semicircular pool with a radius of 339 m mentioned by Fay (2003), suggesting that  $\partial \bar{\delta} / \partial r \approx 0$ . Combination of Eqs. (5) and (6) gives the deceleration (m/s<sup>2</sup>) of a material particle where the energy of the fluid deployed from the cargo tank is transferred to the pool spreading on the sea, and providing the Eqs. (3) and (4), one has:

$$\frac{Du}{Dt} = \frac{\partial u}{\partial t} + u \frac{\partial u}{\partial r} = 0 \Rightarrow -\frac{\partial u}{\partial t} = u \frac{\partial u}{\partial r} \quad (8)$$

Besides the Eq. (8), Fay (2003) defines a time scale,  $t_d$  (s) that determines the time elapsed of the outflow from the cargo tank tear. Orifice models state that the magnitude of the outflow velocity through the tear at, or close to and above the water line is  $\sqrt{gh_0}$  (m/s), so that the magnitude of the outflow volumetric flow rate of spilled LNG is given by  $\sqrt{gh_0} A_h$  (m<sup>3</sup>/s). When multiplied by the discharge time,  $t_d$  (s), gives a volume that, from the mass conservation, must be equal to the volume discharged  $V_0 = A_t h_0$  (m<sup>3</sup>). The initial value of  $h(t)$  (m) inside the cargo tank is  $h_0$ , and both of them are measured from above the waterline, as depicted in Fig. 1. By the time rupture occurs, the carrier is supposed to be loaded at full capacity, operating in quiescent waters of a terminal. The whole cargo is assumed to be held in a carrier equipped with membrane or prismatic cargo tanks of constant cross sectional area,  $A_t$  (m<sup>2</sup>). A number of simplifying hypotheses are here assumed, which includes neglecting the occurrence of phenomena such as: (i) ullage pressure inside the cargo tank, usually less than ~115 kPa (Qiao, 2006); (ii) vacuum breaker and air entering the cargo tank through the breach; as well as (iii) rapid phase transitions, as a result of cryogenic thermodynamic flash due to eventual water entrance into the cargo and ballast tanks during the spill. Cargo tank pressure effects are considered as of low to medium importance (MKOPSC, 2008) on the prediction of liquid outflow from the ship, although it could be considered as being altered due to the potential pressure changes associated with the LNG release, flash of LNG, heat ingress through the inner tank walls, etc. (MKOPSC, 2008; Lehr, 2007). Therefore,

$$t_d \approx \frac{A_t h_0}{\sqrt{gh_0} A_h} = \left( \frac{A_t}{A_h} \right) \sqrt{\frac{h_0}{g}} \quad (9)$$

The pool of LNG evaporates by a boiling and/or fire process and the deployment cannot take place in a time shorter than  $t_d$  (s). The rate of depletion may be thought as expressed by a vaporization (or regression) velocity  $\langle \dot{y} \rangle$  (m/s), function of the mechanisms that vaporizes the cryogenic fluid. Fay (2003) defines the following equations for pool radius for the variation with time of the discharge process from the carrier cargo tank, and subsequent pool formation and evaporation,  $V_p$  (m<sup>3</sup>) as being the volume of the maximum semicircular pool area,  $A_{psc}^{max}$ , (m<sup>2</sup>), it leads to

$$-\left[ \frac{\partial}{\partial t} (h A_t) \right]_{A_h, \langle \dot{y} \rangle} = \sqrt{2gh} A_h \quad (10)$$

$$\left(\frac{\partial V_p}{\partial t}\right)_{A_h, \langle \dot{y} \rangle} = \sqrt{2gh} A_h - \langle \dot{y} \rangle A_{psc}^{max} \quad (11)$$

$$\left[\frac{\partial(\pi R^2/2)}{\partial t}\right]_{A_h, \langle \dot{y} \rangle} = \left(\frac{\partial R}{\partial t}\right)_{A_h, \langle \dot{y} \rangle} = \left(\frac{\beta}{\pi}\right) \sqrt{2\pi g V_p \Delta} \quad (12)$$

The system of partial differential equations (3), (10), (11) and (12) define, therefore, the time history of the discharge from the carrier cargo tank and the subsequent formation and vaporization of the semicircular pool. With equations (12) to (15) correlating density effects and the carrier geometry, with  $\rho_w$  being the sea water mass density (kg/m<sup>3</sup>), one has

$$V_0 = A_i h_0 \quad (13)$$

$$CTV = CTC/n \quad (14)$$

$$A_i = 0.5192(CTV/DR) \approx 0.52(CTV/DR) \quad (15)$$

The parameter  $CTV$  is the cargo tank volume (m<sup>3</sup>), whereas  $CTC$  is the cargo vessel capacity (m<sup>3</sup>);  $n$  is the quantity of tanks of the LNG carrier,  $DR$  is the draft, the vertical distance (m) between the waterline and the bottom of the carrier's hull (keel). Some input data were also proposed by Fay (2003), such as a axi-symetrical pool spread pool dimensionless parameter,  $\beta = 4\sqrt{3} = 2.31$ , experimental vaporization velocity  $\langle \dot{y} \rangle = 0.0008$  m/s, the ship draft  $DR = 11.8$  m as the distance between the ship's keel and the liquid surface, the capacity of cargo vessel  $CTV = 125,000$  m<sup>3</sup>,  $CTC = 125,000/5$  m<sup>3</sup> for each one of the  $n = 5$  cargo tanks,  $h_0 = 13$  m and  $\Delta = 0.58$ . Another dimensionless flow parameter,  $\Phi$ , as a function of  $\beta$ ,  $\Delta$ ,  $\langle \dot{y} \rangle$  and the cargo tank geometry,  $h_0$  (m),  $A_t$  (m<sup>2</sup>) and  $A_h$  (m<sup>2</sup>) was developed:

$$\Phi = \beta \sqrt{2\pi\Delta} \langle \dot{y} \rangle \sqrt{\frac{h_0 A_t^{3/2}}{g A_h^2}} \quad (16)$$

For  $\Phi > 30$ , dimensionless asymptotic values of 2.828, 1.414 and 4 for  $a^{*,max}$  and  $t_v^*$  and  $a^{*,max} \cdot t_v^*$ , respectively, are used. However, for  $\Phi$  values within 1/3 and 30, differently to Fay (2003), the present work proposes, as an approximation, the use of continuous functions to calculate  $\Phi$  within that interval, as follows:

$$a^{*,max} = 0.43 \ln \Phi + 1.184 \quad (17)$$

$$t_v^* = 0.81\Phi^2 - 2.7431\Phi + 3.6982 \quad (18)$$

If the maximum semi-circular pool area,  $A_{psc}^{max}$  in (m<sup>2</sup>) and vaporization time  $t_v$  (s) are expressed in terms of dimensionless variables,  $a^{*,max}$  and  $t_v^*$  and  $\Phi$ , one has (Fay, 2003):

$$A_{psc}^{max} = \left(\frac{A_h \sqrt{gh_0}}{\langle \dot{y} \rangle}\right) a^{*,max} = \left[\frac{\beta^2 (2\pi\Delta) g (h_0 A_t)^3}{\langle \dot{y} \rangle^2}\right]^{1/4} \frac{a^{*,max}}{\sqrt{\Phi}} \quad (19)$$

$$t_v = \left(\frac{A_t}{A_h}\right) \sqrt{\frac{h_0}{g}} t_v^* = \left[\frac{h_0 A_t}{\beta^2 (2\pi\Delta) g \langle \dot{y} \rangle^2}\right]^{1/4} t_v^* \sqrt{\Phi} \quad (20)$$

As per Fay's (2003) model, the critical value of the flow parameter occurs when  $\Phi = \Phi_{cr} = 1.784$ . At this critical point, the flow through the tear transits from slow to fast, respectively, with small and large dimensions of the carrier's hull breaches. Therefore, critical values of  $A_h$ ,  $A_{psc}^{max}$  and  $t_v$ , can be calculated as follows:

$$A_{h_{cr}} = 0.749 \left[ \frac{\beta^2 (2\pi\Delta) \langle \dot{y} \rangle^2 h_0 A_t^3}{g} \right]^{1/4} \quad (21)$$

$$A_{p_{sc,cr}}^{max} = 1.071 \left[ \frac{\beta^2 (2\pi\Delta) g (h_0 A_t)^3}{\langle \dot{y} \rangle^2} \right]^{1/4} \quad (22)$$

$$t_{v_{cr}} = 1.889 \left[ \frac{h_0 A_t}{\beta^2 (2\pi\Delta) g \langle \dot{y} \rangle^2} \right]^{1/4} \quad (23)$$

Upper and lower limits can also be calculated for the case of instantaneous spills when  $\Phi$  approaches 0, providing that  $\beta = 4/\sqrt{3} \approx 2.31$ . Therefore, according to Fay (2003), one has, in (m<sup>2</sup>) and (s), respectively:

$$A_{p_{sc,ub}}^{max} \leq 2.58 \left[ \frac{g\Delta (h_0 A_t)^3}{\langle \dot{y} \rangle^2} \right]^{1/4} \quad (24)$$

$$t_{v_{lb}} \geq 0.785 \left( \frac{h_0 A_t}{g\Delta \langle \dot{y} \rangle^2} \right)^{1/4} \quad (25)$$

As the pool combustion model uses circular pools, a transition from semicircular to circular is necessary. Mass, momentum and energy are supposed to be conserved, so one has  $A_{p_{sc}}^{max} = A_{p_{ci}}^{max}$  (m<sup>2</sup>) (MKOPSC, 2008), and then:

$$A_{p_{sc}}^{max} = A_{p_{ci}}^{max} \Rightarrow D_{p_{ci}} = \frac{1}{\sqrt{2}} D_{p_{sc}} \quad (26)$$

### 3.2 Non-premixed turbulent combustion pool fire

The multi-zone model is based on the model of TMS (2006), also reported in Raj (2007b) and Fay (2006), where the thermal plume models consider that its ‘visible’ height as depicted in Fig. 2.

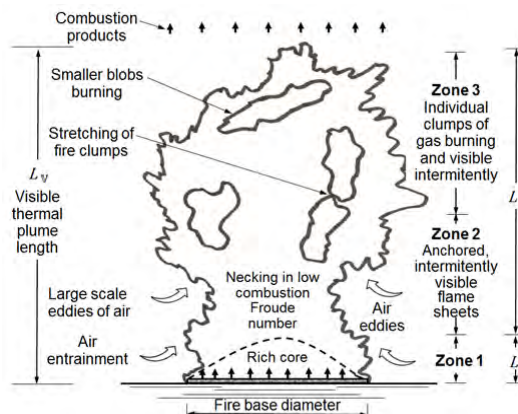


Figure 2 – Thermal plume. Source: Adapted from Raj (2007b).

The plume is composed by three zones.  $L_c$  (m) (bottom), where the combustion is considered to be ‘clean’;  $L_i$  (m) (intermittent, with two zones), where the plume pulsates intermittently; and the highest part which contains its tips, where combustion products are taken off from the fire column by buoyancy. The tips are a time averaged geometric loci

of the visible height of the thermal plume. The three zones added form the ‘visible’ plume length,  $L_V$  (m) which is its time average height. The plume fire base diameter (m) is,  $D_{pci}$  calculated by Eqs. (19) and (26).

### 3.2.1 Model equations

Based on the mass conservation of the chemical species (Warnatz et al. 1999), the equation for the conservation of the (dimensionless) reaction mixture fraction scalar (passive scalar),  $\xi$ , is independent of the choice of chemical elements. For non-premixed turbulent flames with chemical equilibrium and with the flow of the mass center of the mixture control volume being transported by the velocity vector field,  $\mathbf{u}$ , it can be written that

$$\underbrace{\frac{\partial(\rho\xi)}{\partial t}}_{\text{Temporal rate of change of the passive scalar per unit of volume}} + \underbrace{\frac{\partial(\rho\xi)}{\partial x_i} u_i}_{\text{Convective rate of transport of the passive scalar per unit of volume}} - \underbrace{\frac{\partial^2(\rho\mathcal{D}\xi)}{\partial x_i^2} u_i}_{\text{Diffusive rate of transport of the passive scalar per unit of volume}} = 0 \quad (27)$$

If all the molecular diffusivities ( $\text{m}^2/\text{s}$ ) of the reactive mixture,  $\mathcal{D}$ , and the densities,  $\rho$ , are approximately the same for all the species, the passive scalar is independent of the chemical elements,  $k$ , but depends linearly on mass fraction (-) of chemical species,  $w_s$ . In the same fashion, as the element mass fraction (-),  $Z_k$ , the mixture fraction scalar,  $\xi$ , does not have neither source term nor sink term. Therefore, it is conserved during the combustion reactions (passive scalar or conserved scalar). According to Warnatz et al. (1999), the mass fraction of the chemical species (-),  $w_s$ , keeps an approximately linear relationship with the mixture fraction, so that  $w_s \approx w_s(\xi)$  is used to simplify the description of non-premixed turbulent flames. Based on this, the enthalpy and temperature fields can be modeled by the mixture fraction scalar, via  $h$  the specific enthalpy (J/kg), such as

$$\xi = \frac{h - h_{ox}}{h_v - h_{ox}} \quad (28)$$

where  $h_{ox}$  is the oxidizer specific enthalpy (J/kg),  $h_v$  is the fuel vapor specific enthalpy (J/kg). Consistently the mass fraction of the combustion products is correlated to the temperature, via the mixture fraction scalar as follows

$$w_s = w_s(\xi) \equiv w_{prod}(\xi) = \frac{T - T_a}{T_{ad} - T_a} \quad (29)$$

In Eq. (29),  $T$  is the absolute temperature (K),  $T_a$  is the air dry bulb temperature (K) of the atmospheric air outside the flame, and  $T_{ad}$  is the flame (Fay, 2006). It shows that  $w_{prod}(\xi)$  is correlated and computed to  $T$  through  $\xi$ , hence, the non-premixed turbulent flame modeling problem is to track  $\xi$ , for homogeneous chemical species and enthalpies. The pool vaporization process, expressed by one single and global parameter, the overall vaporization mass flow rate of the cryogenic liquid fuel per unit of pool area,  $\dot{m}_v''$ , in  $\text{kg}/(\text{m}^2 \text{ s})$ , receives two contributions: heat transfer from the sea water to LGN and from radiation of pool fire within the plume, both also in  $\text{kg}/(\text{m}^2 \text{ s})$ , i.e.,

$$\dot{m}_v'' = \dot{m}_b'' + \dot{m}_r'' \quad (30)$$

It means, respectively, boiling mass flow rate of the cryogenic liquid fuel and the radiation mass flow rate of this cryogenic (LNG). The relationship between the average vaporization velocity,  $\langle \dot{y} \rangle$ , defined by Eq. (11), and the vaporization mass flow rate [ $\text{kg}/(\text{m}^2 \text{ s})$ ],  $\dot{m}_v''$ , is given, for example, by ABS (2004) as

$$\dot{m}_v'' = \langle \dot{y} \rangle \rho_l \quad (31)$$

The experimental values of  $\dot{m}_v''$  and  $\langle \dot{y} \rangle$  used in the present work have been acquired for  $\langle \dot{y} \rangle$ , in (m/s) from Esteves and Parise (2013). Conversion between  $\langle \dot{y} \rangle$  and  $\dot{m}_v''$  was carried out with Eq. (31), assuming the cryogenic liquid density as  $\rho_l = 422.5 \text{ kg}/\text{m}^3$  for LNG at normal liquid boiling temperature of  $T_b = 111.7 \text{ K}$  at atmospheric pressure at the sea level of  $P_a = 102.3 \text{ kPa}$ , and with (dry bulb) ambient air and water at temperatures of, respectively,  $T_a = 293 \text{ K}$ ,

and  $T_w = 293$  K. The LNG latent heat of vaporization of the cryogenic liquid at these conditions is supposed to be  $\Delta H_{v_l} = 509.3$  kJ/kg (ABS, 2004). The equations used in the model of TMS (2006) and Raj (2007b) are presented next for the thermal plume shown in Fig. 2. Wind effects are calculated by

$$U^* = \frac{U_{wind}}{\left[ (\dot{m}_v'' / \rho_a) g D \right]^{1/3}} \quad (32)$$

where  $U^*$  is the dimensionless ( - ) module of wind velocity vector field,  $U_{wind}$  is the wind velocity (m/s) vector field  $\mathbf{u}$ ,  $\rho_a$  is the density (kg/m<sup>3</sup>) of the atmospheric air outside the plume and  $D$  is a generic fire base (pool) diameter, liquid pool diameter (m). The combustion Froude number is given by

$$Fr_C = \frac{\dot{m}_v''}{\rho_a \sqrt{g D}} \quad (33)$$

Raj (2007b) proposed the following correlations based on experiments for the overall mean height (length) of the 'visible' fire column,  $L_V$ :

$$\frac{L_V}{D} = 5.5 Fr_C^{2/3} \quad \text{for } U^* \leq 1 \quad (34)$$

$$\frac{L_V}{D} = 5.5 Fr_C^{2/3} (U^*)^{-0.21} \quad \text{for } U^* > 1 \quad (35)$$

The wind effects are counterbalanced by the gravitational ones, since the geometry of turbulent diffusion fire plumes is governed by low Froude number, which gives them a low buoyancy profile. Bottom 'clean burning zone' length,  $L_C$ , and ratio  $\psi = L_C/L_V$  was correlated by experimental data acquired from 35 m diameter field tests in Montoir (Malvos and Raj, 2006), finding that  $L_C$  near fire column base was small (about 10 m, or 15 %) when compared to the overall 66 m of the. TMS (2006) and Raj (2007b) developed then the correlations (36) and (37) defining fire plume parameters  $L_C$ ,  $L_V$ ,  $L_I$ ,  $\psi = L_C/L_V$  and  $Fr_C$ :

$$\psi = \frac{L_C}{L_V} = \left( 1 - \frac{L_I}{L_V} \right) = 0.70 + \log_{10} \left[ (Fr_C)^{1/4} \right] \quad (36)$$

$$L_I = (1 - \psi) L_V \quad (37)$$

The attenuation,  $E_s$  (kW/m<sup>2</sup>), on the emitted effective radiation, is due to the dimensionless total hemispheric transmissivity of the smoke,  $\tau_s$ , that reduces the nominal surface emissive power  $E_0$  (kW/m<sup>2</sup>) of the fire near the base of the plume where the 'clean' combustion takes place, giving

$$E_s = E_0 \tau_s \quad (38)$$

The transmissivity depends on the specific extinction area,  $A_C$  (m<sup>2</sup>/kg), soot mass concentration,  $c_s$  (kg/m<sup>3</sup>) and optical beam length (m)  $L_{beam}$ . As the extinction coefficient and the optical beam length in general depend on the wavelength, TMS (2006) and Raj (2007b) proposed the following equation:

$$\tau_s = e^{- (A_C c_s L_{beam})} \quad (39)$$

Raj (2007b) showed that  $c_s$  is related to  $\rho_a$ , to the burnt fuel mass fraction (%)  $Y$  emitted as smoke, to the ratio  $\mathfrak{R} = 17.17$  ( - ) between the stoichiometric entrainment air/vapor of methane, the burning efficiency ( - ) of the fuel  $\gamma$ , the lower combustion heat of the liquid fuel (J/kg-K)  $\Delta H_{C_l}$ , and specific heat at constant pressure (J/kg-K) of the entraining air,  $c_{P_a}$ . Parameter  $C_s$  is given by a correlation proposed by Raj (2007b), as follows

$$C_s = \rho_a Y \frac{1}{1 + (\mathfrak{R}/Y) + \left[ \Delta H_{C_l} / (c_{P_a} T_a) \right]} \quad (40)$$

Raj (2007a,b) recommended also that optical beam length for cylindrical fires,  $L_{beam}$ , should be considered as 63 % of the diameter of the pool fire base, as follows:

$$L_{beam} = 0.63D \quad (41)$$

as long as the soot mass yield per unit mass of fuel burned, should be expressed taking experiments of Notarianni et al. (1993) with petroleum fires with diameters from 1 to 17 m, that proposed an empirical correlation between  $Y$  and  $D$ , given by Eq. (42)

$$Y = 9.412 + 2.758 \log_{10}(D) \quad (42)$$

There is a probability of the fire column surface irradiates in the intermittency zone just above the ‘clean’ combustion zone (consequently  $L_{\parallel} > L_C$ ). In such a case, a probability function,  $p(\chi)$ , can be associated to a fraction between the axial fire length and the mean length (height) of the visible fire plume. This can be also interpreted as the fraction of the time that the outer layers of the cylindrical fire ‘open’ and show the ‘inner core’ of the fire column. Thus, it radiates at the maximum surface emissive power (SEP), and the remainder of the time the emission is from the smoke layers. The order of this polynomial a function is given by the power  $n$ , was calibrated (‘best fit’) to the experiments with the 35 m diameter of ‘Montoir’ LNG fire tests. The value of  $\chi$  is obtained by (TMS, 2006; Raj, 2007b).

$$p(\chi) = 1 \quad \text{for} \quad 0 \leq \chi \leq \psi \quad (43)$$

$$p(\chi) = \left( \frac{1-\chi}{1-\psi} \right)^n \quad \text{for} \quad \psi \leq \chi \leq 1 \quad (44)$$

$$\chi = \frac{Z}{L_{\forall}} = \frac{\text{length along the fire axis}}{\text{visible fire plume length}} \geq \psi \quad (45)$$

From Eqs. (36) and (45),  $\psi = L_C/L_{\forall}$  and  $\chi = Z/L_{\forall}$ , respectively, are geometric parameters and their ratio  $\chi/\psi = Z/L_C$ . TMS (2006) and Raj (2007a,b) defined that only a time averaged surface emissive power of visible fire plume ( $\text{kW/m}^2$ ),  $\bar{E}$ , of the nominal SEP of the fire near the base of the plume,  $E_0$ , is irradiated to the outer parts of the fire column, being correlated as follows:

$$\frac{\bar{E}}{E_0} = \psi + \left[ \frac{1+n e^{-\left( A_L C_s L_{beam} \right)}}{1+n} \right] (1-\psi) \quad (46)$$

The value of power  $n$  was determined and adjusted according to experimental data acquired in Montoir LNG fire tests, when  $n = 3$ . The total hemispheric time average emissivity of the fire (wavelength independent),  $\bar{\epsilon}$ , depends on the diameter of the fire column,  $D$  (m), and the spectral optical thickness (optical path length) (m)  $\kappa_{\lambda}$ . Based on optical properties, it is calculated as:

$$\bar{\epsilon} = 1 - e^{-(D/\kappa_{\lambda})} \quad (47)$$

Raj (2007b) used the results of China Lake field tests, acquired with a LNG fire with 13 m diameter, and its optical thickness was calculated as being 13.81 m. Using data from China Lake and Montoir site tests, TMS (2006) determined the maximum emissive power at the base of the fire as being  $325 \text{ kW/m}^2$ , supposedly to be equivalent of a blackbody with temperature of 1,547 K. With these experimental parameters, the fire base emissive power can be calculated, considering the concept that the optical thickness is the inverse of the extinction coefficient,  $\kappa_{\lambda} = 1/\mathcal{L}_{\lambda}$

$$E_0 = E^{max} \underbrace{\left[ 1 - e^{-\left( D_{pci} / \kappa \lambda \right)} \right]}_{=\bar{E}} = E^{max} \left[ 1 - e^{-\left( D_{pci} \mathcal{E} \lambda \right)} \right] \quad (48)$$

4. RESULTS AND DISCUSSIONS

The non-linear algebraic equations were solved using EES® platform. Semicircular pools were investigated with tears varying from  $1 \text{ m}^2 \leq A_h \leq 100 \text{ m}^2$ . Twenty diameters were chosen in this interval and for each one of them,  $t_v$  and  $A_{psc}^{max}$  were determined. A specific tear of  $A_h$  of  $5 \text{ m}^2$  expected to occur in the LNG industry was analyzed with  $\langle \dot{y} \rangle = 0.0008 \text{ m/s}$  to compare with Fay’s (2003) results. Subsequently, two membrane or prismatic carrier geometries were simulated with  $125,000 \text{ m}^3$  and  $265,000 \text{ m}^3$  considering two values of  $\langle \dot{y} \rangle$ , of  $0.00021$  and  $0.0011 \text{ m/s}$ .

4.1 Comparison with existing pool spill/spreading models

4.1.1 Reproduction of results of Fay (2003) ship geometry

Results are presented in Fig. 3,  $A_{psc}^{max}$  and  $t_v$ . A convention is here adopted: light gray color is used for critical values of vaporization time and maximum semicircular pool area, whereas dark gray color for maximum vaporization time and peak of the maximum semicircular pool area.

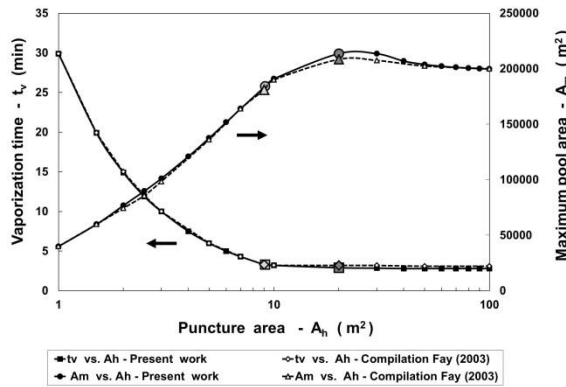


Fig. 3. Comparison of the present work with Fay’s (2003) results. One single  $14,300 \text{ m}^3$  cargo tank spill from a LNG carrier -  $\langle \dot{y} \rangle = 0.0008 \text{ m/s}$ .

Carriers with membrane prismatic tanks of constant cross section were considered, and the agreement of results were good. It suggests that Eqs. (17) and (18) did not influence the accuracy of results, if compared to Fay’s model.

4.1.2 Fay’s Geometry vs. Sandia’s Geometries

Fig. 4 compares Fay’s (2003) and Sandia’s (2008) geometries, for the vaporization velocities above.

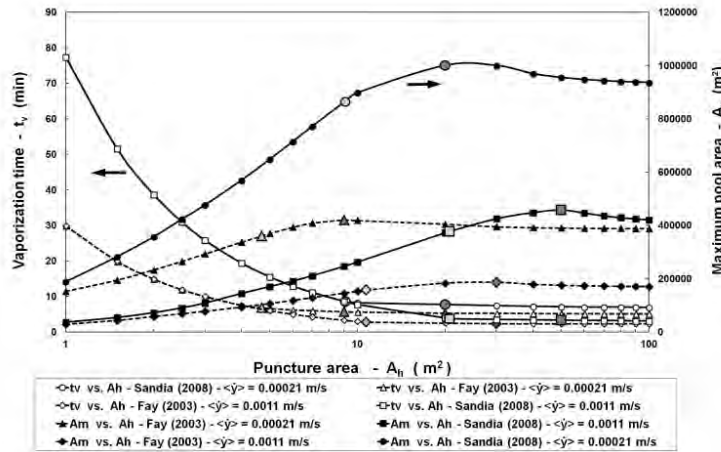


Fig. 4. Fay’s (2003) ( $125,000 \text{ m}^3$ ) vs. Sandia’s (2008) ( $265,000 \text{ m}^3$ ) geometries.

The rise in geometry by a two-fold factor, increases, by far, the maximum size semicircular pools, especially at a lower vaporization velocity (0.00021 m/s). It jumps from around 420,000 m<sup>2</sup> to about 1,000,000 m<sup>2</sup>, from smaller (Fay’s) to the bigger (Sandia’s) geometry. Semicircular pool areas of both Fay’s and Sandia’s geometries, at the lowest puncture (1 m<sup>2</sup>) and slower velocity are about, respectively, 152,000 m<sup>2</sup> and 188,000 m<sup>2</sup>, roughly with the same order of magnitude. With the same puncture and at the fastest velocity, they are significantly smaller with, respectively, 29,000 m<sup>2</sup> and 36,000 m<sup>2</sup>. This is an indication that the size of the pool for smaller tears (‘slow’ disgoring of cryogenic LNG onto the sea) is not very strongly dependent on the tear size and vessel geometries, but rather on the vaporization velocity instead, as expected.

**4.2 Comparison with existing non-premixed pool fire models and experimental data**

*4.2.1 Thermal plume geometry varying with circular pool diameter and combustion Froude number*

Figure 5 presents the computer runs obtained for negligible wind effects ( $U_{wind} \approx 0$ ). It shows the behavior of the ratio  $L_v/D_{pci}$  with diameter, provided by the Eqs. (33) and (34). Circular pool diameters are converted from semicircular format using Eq. (26) covering the interval between 10 m and 500 m, as expected to occur in LNG industrial practice.

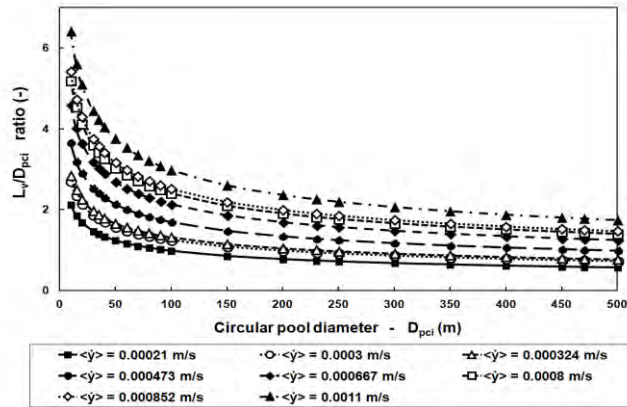


Fig.5. Thermal plume geometry vs. circular pool diameter.

The behavior for the eight velocities followed the same pattern.. But if in lieu of pool diameter, the Froude number is used to describe the profile of the  $L_v/D_{pci}$  ratio, it would have otherwise the format presented in Fig. 6.

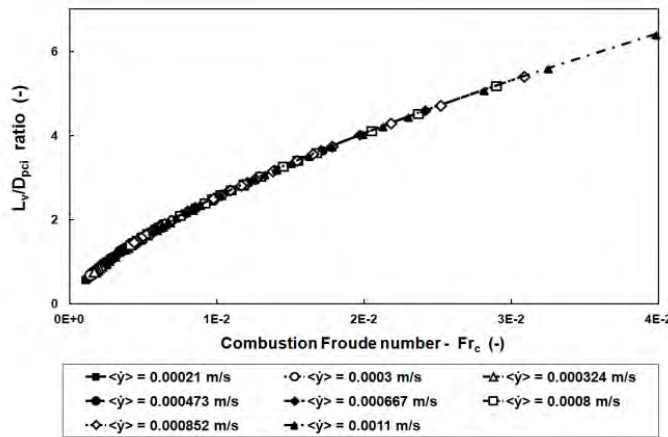


Fig.6. Thermal plume geometry vs. combustion Froude number.

One can determine the overall interval between the diameters of 500 m and 10 m for each one of dimensionless groups, i.e.,  $0.00107 \leq Fr_C \leq 0.03985$  and geometry, varying accordingly,  $0.57752 \leq L_v/D_{pci} \leq 6.41707$ . Using either Fig. 5 or Fig. 6, the higher the velocity is, the higher the Froude number and the geometry will be, forming taller plumes for the same diameter. Therefore,  $L_v/D_{pci}$  depends strongly on the  $Fr_C$  as depicted in Fig. 6. This trend the fire to produce more and more soot, reducing the surface emissive power of the column, so larger diameters usually produce more smoky and less harmful plumes, since its time average surface emissive power lowers as the diameter raises as previously demonstrated.

#### 4.2.2 Surface emissive power varying with circular pool diameter and vaporization velocity

Circular pool fires with diameters of 15, 20, 35, 100 and 300 m were simulated. The predicted behavior of  $Fr_C$ ,  $Y$ ,  $C_s$ ,  $\psi$ ,  $\tau_s$  and  $\bar{E}$  as functions of  $D_{p_{ci}}$  was verified, and in general they were coincident with original findings from Raj (2007a,b) and TMS (2006). Overall, agreement with available literature and experimental data of  $\bar{E}$ , from TMS (2006) and Raj (2007b) and present work, was reasonable. Summarized results are presented: (i) For  $D_{p_{ci}} = 15$  m: 172 kW/m<sup>2</sup> (TMS, 2006; Raj, 2007b) and 185-224 kW/m<sup>2</sup> (Raj et al. 1979) of China Lake tests vs. 171 kW/m<sup>2</sup> of the present work; (ii) for  $D_{p_{ci}} = 20$  m: 183 kW/m<sup>2</sup> (Raj, 2007b) and 140-180 kW/m<sup>2</sup> (Mizner and Eyre, 1982) for large scale LNG pool fires vs. 184 kW/m<sup>2</sup> of this work; (iii) for  $D_{p_{ci}} = 35$  m: 177 (Raj, 2007b) and  $175 \pm 30$  kW/m<sup>2</sup> (Malvos and Raj, 2006) of Montoir tests vs. 178 kW/m<sup>2</sup> presented in this paper; (iv) for  $D_{p_{ci}} = 100$  m: 113 kW/m<sup>2</sup> (Raj, 2007b) vs. 113 kW/m<sup>2</sup> as predicted with the present simulations; (v) for  $D_{p_{ci}} = 300$  m [estimated pool size due to spill of 1/2 cargo tank content (12,500 m<sup>3</sup> of LNG) from an LNG carrier]: 90 kW/m<sup>2</sup> (Raj, 2007b) vs. 89 kW/m<sup>2</sup> as simulated in the present study.

#### 4.3 Coupling of spill and spreading and non-premixed turbulent pool fire models

An overall coupling was made with both models, encompassing both geometries of Fig. 4 considering  $D_h$  of 1 and 5 m, and  $\langle j \rangle$  of 2.1E(-4), 3.24E(-4), 8E(-4) and 11E(-4) m/s. All relevant parameters,  $t_d$ ,  $t_v$ ,  $A_{p_{sc}}^{max}$ ,  $D_{p_{sc}}$ ,  $D_{p_{ci}}$ ,  $Fr_C$ ,  $L_C$ ,  $L_N$ ,  $\psi$ ,  $L_N/D_{p_{ci}}$ ,  $C_s$ ,  $\tau_s$  and  $\bar{E}$ , were simulated consistently and without any discontinuity for the two geometries of carriers with membrane or prismatic tanks, varying with two-fold capacities. Results for both geometries with the lowest vaporization velocity were, respectively, (i) Fay (2003): 27.1 min; 38.3 min; 118,560 m<sup>2</sup>; 549 m; 388 m; 0.001221; (-); 244 m; (-); 0.63; 4.26E(-4) kg/m<sup>3</sup>; 1.3E(-6); 74 kW/m<sup>2</sup> and Sandia (2008): 70.1 min; 99.1 min; 147,056 m<sup>2</sup>; 612 m; 423 m; 0.001156; (-); 262 m; (-); 0.61; 4.3E(-4) kg/m<sup>3</sup>; 2.7E(-7); 73 kW/m<sup>2</sup>.

### 5. CONCLUSIONS

The following conclusions can be postulated: (1) More than 20 orifice models published since 1969, as well as several types of pool fire models were reviewed: punctual source flame, solid flame, integral, multi-zones, field (CFD). To the authors' knowledge, no work has been published to the present date coupling, explicitly, models of spill and spreading and turbulent diffusion pool fire; (2) A comprehensive survey of experimental data for  $\langle j \rangle$ , since 1978, has been presented; (3) Results attest the robustness of both models. The present work covered spill and spreading with tears between 1 and 100 m<sup>2</sup>, possible to occur at in the current LNG industry, testing 20 hole diameters with 8 velocities. The turbulent diffusion fire model covered circular pools from 1 to 500 m diameter, with 50 different diameters and 8 vaporization velocities. The model proved to be robust and reliable, simulating all the relevant phenomena and important mechanisms; (4) The flow parameter,  $\Phi$ , was adjusted by Eqs. (17) and (18) in the interval 1/3 to 30, using a continuous 'best fit' adjustment. Results indicated that this adjustment did not affect substantially the values obtained; (5) When compared to experimental measurements of mean SEP from NAR radiometers along the plume axis, the model reproduced well the experiments of China Lake, large scale LNG pool fires and Montoir field experiments.

### 6. REFERENCES

- ABS Consulting Group. Consequence Assessment Methods for Incidents Involving Releases from Liquefied Natural Gas Carriers. Washington, DC: 2004, May, 56 p. Technical Report to FERC, 131-04 GEMS 1288209.
- Blanchat, T., Helmik, P., Jansen, R., Luketa, A., Deola, R., Suo-Anttila, J., Mercier, J., Miller, T., Ricks, A., Simpson, R., Demosthenous, B., Tieszen, S., Hightower, M., The Phoenix Series Large Scale LNG Pool Fire Experiments, in: Sandia National Laboratories (Ed.), Sandia Report SAND2010-8676, U.S. Department of Energy, Washington, DC; Albuquerque, NM; Livermore, CA, December 2011.
- Esteves, A.S., Parise, J.A., Mathematical modeling of cryogenic spills onto quiescent sea waters followed by pool fires of Liquefied Natural Gas (LNG), Applied Thermal Engineering 59 (2013) 587-598.
- Fay, J.A., Model of Large Pool Fires. Journal of Hazardous Materials, B136:219-232, 2006.
- Fay, J.A., Model of Spills and Fires from LNG and Oil Tankers. Journal of Hazardous Materials, 96:171-188, 2003.
- Fay, J.A., Spread of Large LNG Pools on the Sea. Journal of Hazardous Materials, 140:541-551, 2007.
- Hissong, D.R., Keys to Modeling LNG Spills on Water. Journal of Hazardous Materials, 140:465-477, 2007.
- Hoult, D.P., Oil Spreading on the Sea. Annual Review of Fluid Mechanics, 4:341-368, 1972.
- Johnson, A.D., A Model for Predicting Thermal Radiation Hazards from Large-Scale LNG Pool Fires. In: Major Hazards Onshore and Offshore, IchemE Symposium Series No. 130, European Federation of Chemical Engineers (EFCE) Event No. 470, EFCE Publication No. 93, 507-524, 20-22 October 1992, Manchester, UK.

- Lees, F.P., Loss Prevention in Process Industries, Hazard Identification, Assessment and Control. 2nd ed. Butterworth-Heinemann, 3.000 p., 1996, Oxford, UK.
- Lehr, W.J., Unique Physics of LNG Spills, Proceedings of the Thirtieth AMOP Technical Seminar, Environment Canada, Ottawa, ON, pp. 637-644, 2007.
- Luketa-Hanlin, A., A Review of Large-Scale Spills: Experiments and Modeling. *Journal of Hazardous Materials*, A(132):119-140, 2006.
- Malvos, H., Raj, P.K., Details of 35 m Diameter LNG Fire Tests Conducted in Montoir, France In 1987 and Analysis of Fire Spectral and Other Data. The 2006 Spring National Meeting of the AIChE, Session T6005 LNG VI, Risk & Safety, Orlando, FL, April 2006.
- Mizner, G.A., Eyre, J.A., Large scale LNG and LPG pool fires, in: Proceedings of the Institution of Chemical Engineering Symposium, Series 71, Manchester, April, 1982.
- MKOPSC, Mary Kay O'Connor Process Safety Center. Pool spreading description. In LNG Pool Fire Modeling White Paper, CLNG Workshop on LNG Pool Fire Modeling. Mary Kay O'Connor Process Safety Center, College Station, TX, September 2008.
- Notarianni, K.A., Evans, D.D., Walton, W.D., Madrzykowski, D., Lawson, J.R., Smoke Production from Large Oil Pool Fires. Proceedings of the Interflam 1993 Fire Safety International Fire Conference, Interscience Communications Ltd London, 111-119. March 1993, Oxford, UK.
- Oka, H., Consequence Analysis of Large-Scale Liquefied Natural Gas Spills on Water, in: Primoz Potocnik & InTech (Eds.), Natural Gas, National Maritime Research Institute, Croatia, Japan, 2010, pp. 549-570.
- Pula, R., Khan, F.I., Veitch, B., Amyotte, P.R., Revised Fire Consequence Models for Offshore Quantitative Risk Assessment. *Journal of Loss Prevention in the Process Industry*, 18:443-454, 2005.
- QATARGAS, "Mozah", The world's largest LNG vessel, The Pioneer, The magazine of Qatar Operating Company Limited, July-August 2008, Issue No. 120.
- Qiao, Y., West, H.H., Mannan, M.S., Jonhson, D.W., Cornwell, J.B., Assessment of the Effects of Release Variables on the Consequences of LNG Spillage onto Water Using FERC Models. *Journal of Hazardous Materials*, 130:155-162, 2006.
- Raj, P.K., LNG Fires: a Review of Experimental Results, Models and Hazard Prediction Challenges. *Journal Hazardous Materials*, 140:444-464, 2007a.
- Raj, P.K., Mudan, K.S., Moussa, A.N., Experiments Involving Pool and Vapor Fires from Spills of LNG on Water. Report #CG-D-55-79, NTIS AD077073, U.S. Coast Guard (USCG), Washington, DC 20590, 1979.
- Raj, P.K., Large Hydrocarbon Fuel Pool Fires, Physical Characteristics and Thermal Emission Variations with Height. *Journal of Hazardous Material*, 140:280-292, 2007b.
- Rew, P.J., Spencer, H., Madison, T., Sensitivity of Risk Assessment of Flash Fire Events to Modeling Assumptions. Institution of Chemical Engineers (IChemE) Symposium Series, 144:265-278, 1998.
- Sandia National Laboratories, Breach and Safety Analysis of Spills Over Water from Large Liquefied Natural Gas Carriers. Washington, DC; Albuquerque, NM; Livermore, CA: U.S. Department of Energy, May 2008, Technical Report SAND2008-3153.
- Sandia National Laboratories. Guidance on Risk Analysis and Safety Implications of a Large Liquefied Natural Gas (LNG) Spill Over Water. Washington, DC; Albuquerque, NM; Livermore, CA: U.S. Department of Energy, December 2004, Technical Report SAND2004-6258.
- The Federal Energy Regulatory Commission (FERC). Notice of Availability of Staff's Responses to Comments on the Consequence Assessment Methods for Incidents Involving Releases from Liquefied Natural Gas Carriers. Washington, DC: Docket No. AD04-6-000, June 2004.
- TMS. Technology & Management Systems, Inc. Spectrum of Fires in a LNG Facility - Assessments, Models and Consideration in Risk Evaluations. Burlington, MA: The U.S. Department of Transportation Pipeline & Hazardous Materials Safety Administration, 2006, Final Technical Report, 99 p.
- Vachon, M., Champion, M., Integral Model of a Flame with Large Buoyancy Effects. *Combustion and Flame*, 63, 269-278, 1986.
- Warnatz, J., Maas, U., Dibble, R.W., Combustion – Physical and Chemical Fundamentals, Modeling and Simulation, Experiments, Pollutant, Formation, 2nd ed. 1999, Springer-Verlag, Berlin/Heidelberg.

## 7. RESPONSIBILITY NOTICE

The authors are the only responsible for the printed material included in this paper.

## 8. ACKNOWLEDGEMENTS

The authors are indebted to CNPq (from the Brazilian Ministry of Science and Technology) and to FAPERJ (State of Rio de Janeiro Research Funding Agency) for the financial support.